Magazine of Civil Engineering

ISSN 2712-8172

journal homepage: http://engstroy.spbstu.ru/

Research article

UDC 624.016

DOI: 10.34910/MCE.129.2

Cable roof with stiffening girder and flexible membrane shell

A.V. Chesnokov ✉ , ***V.V. Mikhailov***

Lipetsk State Technical University, Lipetsk, Russian Federation

✉ *andreychess742@gmail.com*

Keywords: steel beam, steel girder, high strength steel, composite materials, structural design, stiffness, pre-stressed cable systems, tensile membrane roofs

Abstract. The framework of the roof, considered in the research, is a two-chord truss-like structure. The chords are joined by vertical struts. They are made of high-strength steel cables. A flexible polymer membrane is attached to the restraining chord. The opposite supports of the roof are joined by a girder made of ordinary structural steel. The girder mitigates deformations of the truss under non-uniform external loads. It is loosely connected to the vertical struts. The loose connections (so-called design clearances) prevent overstressing the girder by uniform impacts. Computational technique for static analysis of the cable roof is proposed. The main structural parameters are estimated under the condition of the full use of the material properties. The bearer chord reaches the ultimate limit state under the uniformly distributed transverse load, which is taken by the cable truss in full. A non-uniform impact is split between the truss and the girder by the condition of compatibility of deformations. The expressions for the axial stiffnesses of the chords, the design clearance values, and the allowable deformations of the roof are given. The work contributes to the development of hybrid building constructions by providing the initial data for the conceptual design stage. It allows to validate structural models and to verify the results of numerical computer analysis.

Citation: Chesnokov, A.V., Mikhailov, V.V. Cable roof with stiffening girder and flexible membrane shell. Magazine of Civil Engineering. 2024. 17(5). Article no. 12902. DOI: 10.34910/MCE.129.2

1. Introduction

The framework of the roof, considered in the research, is a two-chord cable truss with a girder arranged between the opposite supports. The chords are joined by vertical struts (Fig. 1). The struts are loosely connected to the girder: the truss moves freely by design clearances before the girder begins taking external transverse loads.

The truss is pre-stressed by tensioning the bearer chord '*b*', which is situated below the restraining chord '*r*'. The flexible shell is attached to the restraining chord. It is made of architectural fabrics or a polymer membrane [1].

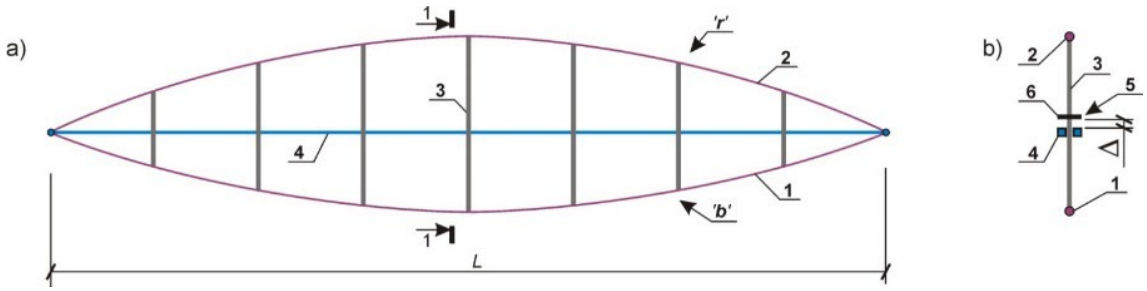

Figure 1. The framework of the roof structure considered in the research: a – general view, b – view along the line 1-1; 1 – bearer chord 'b'; 2 – restraining chord 'r'; 3 – vertical strut; 4 – stiffening girder; 5 – loose connection of the strut and the girder (design clearance); 6 – retainer.

The roof can be split into separate sections. An ordinary section is encompassed by catenary and backstay cables (Fig. 2). The section, considered in the research, is highlighted in blue in Fig. 2.

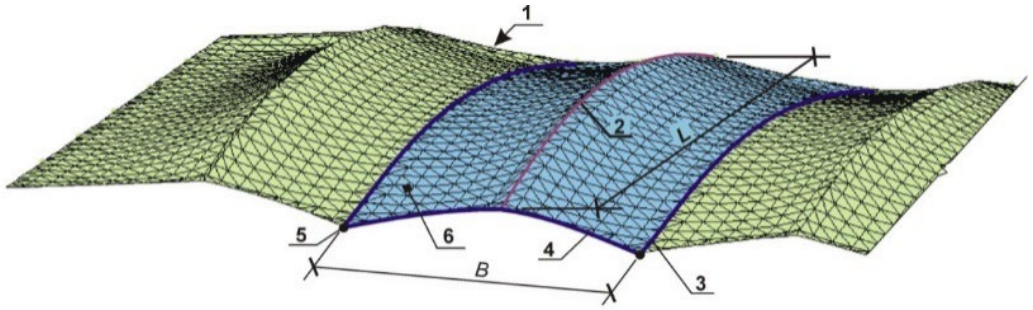

Figure 2. The shell of the roof: 1 – the flexible membrane; 2 – ridge, formed by the restraining chord of the roof's framework; 3 – backstay cable; 4 – catenary cable; 5 – fixed support; 6 – roof's section, considered in the research.

Pre-stressed cable structures with flexible shell belong to hybrid building constructions. They are an efficient solution for sheltering urban spaces, exhibition halls, airports, railway stations, and stadiums, as well as for temporary covering archeological areas, sites of architectural heritage and emergency facilities [2–6].

The key factor, which stimulates the growth of popularity of the hybrid constructions, is the emergence of high-quality steel cables and polymer membranes in the market. Development of multifunctional structural membranes offers great opportunities for self-sensing envelopes of buildings, as well as in the field of energy harvesting and storage [7]. Being far superior to the ordinary building materials, the cables and the membranes are a competitive solution in spite of relatively high cost.

Cable and membrane structures, however, exhibit complex behavior under load. Kinematic displacements, brought about by non-uniform external impacts, can far exceed deflections by uniform loads of higher intensity [8]. Thus, the limit state of serviceability is violated. It prevents the full use of strength properties of structural materials and requires further enhancement of the design solutions.

In order to reduce the deformations, cable structures are combined with rigid threads and stiffening girders. Load-carrying behavior of a suspended roof structure with lattice threads is analyzed in [9]. Arrangement of a stiffening girder between the opposite supports of cable structures is transferred from the bridge engineering [10]. The girder is suspended by the cables, which reduce its material capacity. The cable spacing is investigated by means of static and dynamic analysis of cable-stayed bridges [11].

Horizontal cantilever girders, supported by guy cables, form the bearer framework for the roofs of small capacity stadiums [12]. Such a solution, however, suffers from the uplift wind loads, which can cause slackening of the cables and overstress the cantilever.

The stiffening girders, being embedded into the cable structures, form strutted systems [13]. In addition to the effective mitigation of the deflections, the girders bear the thrust brought about by the flexible chords of the construction thus preventing overstress of the supporting structures.

The strutted systems have found use for radio transmitting towers, providing reduction of cost up to 50 % [14]. The girder, being arranged in the vertical direction, serves as a lightweight mast or a pole for supporting temporary building constructions, such as awnings and tents [15, 16].

Deformability of the strutted systems is decreased by means of multilevel arrangement of the cable chords [13], as well as by transforming the top chord into a secondary cable truss with inclined web ties

[17, 18]. The secondary truss results in reduction of the vertical displacements by 32 % in comparison to a single cable [19].

A common disadvantage of the strutted systems is that the girder, being of high relative stiffness, becomes overstressed by external transverse loads, while high-strength chords of the cable truss remain underused. Mitigation of the stresses in the structural elements is achieved by means of passive adaptation strategy. The passive adaptation means, that the structural compliance is implemented into the structural behavior [20].

Design clearances, which allow the structural elements to move freely a certain distance, can be considered as the means for the passive adaptation. An emergency-proof girder structure is proposed and optimized in [21, 22]. The girder transforms into a truss-like structure in case of failure of the middle support. The transformation is performed using loosely connected structural elements.

The solution [23] allows the girder to bear only its own weight in the transverse direction until the design clearances are exhausted. It contributes to more efficient stress redistribution in the construction, because the flexible chords, made of high-strength steel cables, take the major portion of the external impacts.

Structural analysis of the hybrid building constructions, which include flexible cable and membrane elements, must take into account complex nonlinear behavior under load. Pseudo linear approach, based on replacing of the flexible catenaries with trussed elements, is not appropriate [24]. Numerical methods are commonly used for geometrically nonlinear structural analysis. They allow thorough consideration of the external loads and provide detailed information on the stress and force distribution in the structural members.

A two-step numerical strategy for the static analysis of cable structures is proposed in [25]. The initial stresses in the cables and the reference configuration of the structure is determined by the catenary force density method. The convergence of the numerical analysis is achieved by the iterative Newton–Raphson method.

The mixed algorithm for nonlinear analysis of hybrid structures made of cable and rigid (truss) elements is proposed in [26]. The equilibrium is achieved iteratively by the secant method.

In [27] point based iterative approach is used for geometrically nonlinear analysis of cable trusses and nets. Such an approach, in comparison to similar methods of structural analysis, requires much less computational resources.

The design process of the flexible membranes, which form the shell of the hybrid buildings, is considered in [28]. The equilibrium shape of the flexible membrane strongly depends on the stress distribution in the surface. The influence of the membrane geometry on the structural behavior of the whole construction is investigated in [29]. Form-finding theories and approaches are considered in [30]. Improved “force density” numerical technique for shape determination of hybrid structures is devised in [31]. The problem of multiple shapes and unstable equilibrium positions is considered in [32].

Coupled analysis of the flexible membrane and the supporting structure is considered in [33–35]. Numerical analysis of the arch structure restrained by the membrane is considered in [36]. Integrated approach, which includes optimization steps, is proposed in [28]. The approach allows finding the intermediate stress-free configuration of the membrane, from which it is stretched, into the desired shape with the appropriate stress distribution [37].

The procedure for the numerical simulation of flexible membrane structures is summarized in [38]. The analysis is based on the finite element method, which is implemented using specialized software packages for nonlinear structural simulation.

Numerical methods, however, require the main structural parameters to be given in advance. Thus, analytical technique is needed to determine stiffness properties of the structural elements and the magnitude of the pre-stressing of the cables and the membranes [39]. Simplified approach is also required for validating structural models and for verifying the numerical results.

The analysis of single cables, cable nets and trusses is considered in [8]. The analytical dependence for the length of the cables is proposed. The cubic equation for determination of the thrust is given. The compatibility of deformations of the chords of the cable trusses is used for the static analysis under load.

The engineering approach for simulating suspension bridges with rigid cables and girders is devised in [40]. The analytical expressions for the thrust induced by the cables, as well as for the vertical deflections at the middle and at the quarter points of the span are derived.

The equilibrium equations for a flexible cable, subjected to self-weight and temperature variations, are given in [41]. The equations are written in the differential form. Having been integrated, they are solved

given the boundary conditions for the cable. This approach is used for analyzing single cables and cable nets.

Analysis of girders with reinforcing flexible ties is considered in [14]. The condition of compatibility of deformations is used for obtaining the deflections and the stress-strain state under load.

According to the literature review, the following gaps in the field of the cable and membrane structures may be highlighted:

- cable truss systems, stiffened with girders, and flexible membrane shells are considered separately. Multistructure integration should be investigated, because the united (hybrid) system is expected to be a competitive design solution;
- structural compliance should be used for improving the structural behavior. Thus, the passive adaptation needs to be implemented into the hybrid roofs;
- simplified solution techniques must be developed for the static analysis of the hybrid constructions, as well as for estimating their main structural parameters.

The purpose of the present work is to devise the computational technique for structural analysis of the cable roofs, stiffened with girders and enveloped with flexible membranes.

The tasks to be solved are the following:

1. To include polymer membrane shell into the structural model of the plane cable truss. To propose the numerical technique for estimating the effective stiffness of the membrane in the model.
2. To propose computational technique for static analysis of the cable truss with the girder and the passive adaptation means in the form of design clearances. To take into account both uniform and non-uniform external loads.
3. To provide analytical expressions for calculation of design clearances, pre-tensioning of cable truss and stiffness properties of the chords under the satisfied limit states conditions.

2. Methods

The structural model of the section of the roof highlighted in Fig. 2 is shown in Fig. 3.

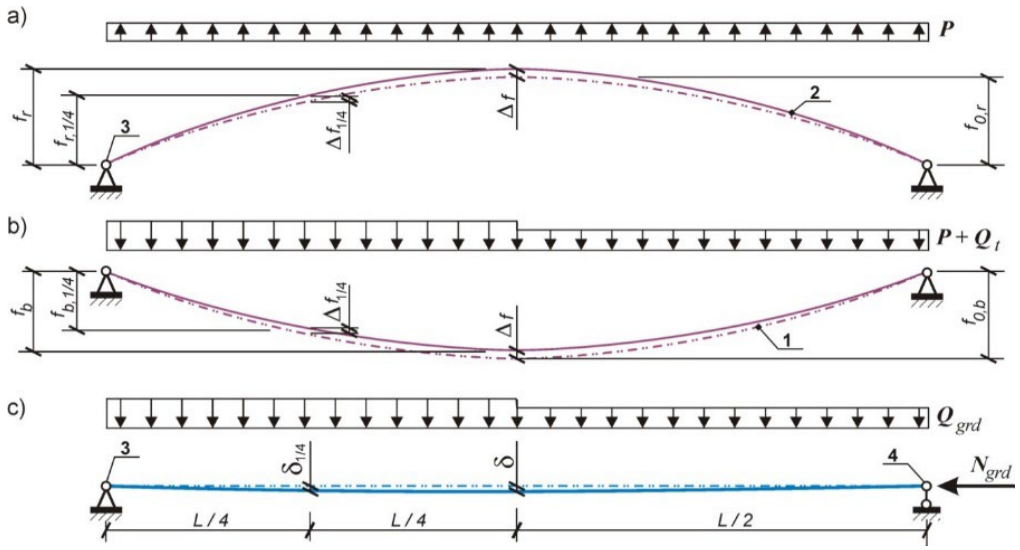

Figure 3. Structural model of the section of the roof: a, b – restraining and bearer chords, respectively, c – the stiffening girder; 1, 2 – initial and deformed positions of the elements, respectively; 3 – fixed support; 4 – support fixed in vertical direction only; P is the link load between the chords; Q_t and Q_{grd} are the external transverse loads on the cable truss and the girder; N_{grd} is the longitudinal load on the girder.

The following assumptions are considered in the present work. No material nonlinearity is present and Hook's law is valid. Longitudinal shortening of the girder under load is negligible, and the roof's span L is stationary. Nodal displacements are allowed only in the vertical direction and the struts between the chords are incompressible. Thus, the rises of the chords f are mutually dependent at the deformed state:

$$f_b = f_{0,b} - \Delta f \tag{1a}$$

$$f_r = f_{0,r} + \Delta f \tag{1b}$$

$$f_{b,1/4} = 0.75 \cdot f_{0,b} - \Delta f_{1/4} \tag{1c}$$

$$f_{r,1/4} = 0.75 \cdot f_{0,r} + \Delta f_{1/4} \tag{1d}$$

where Δf, $\Delta f_{1/4}$ are the displacements of the roof in the center and in the quarter point of the span, respectively; $f_{0,b}$ and $f_{0,r}$ are the initial rises of the parabolic chords.

Only shallow cables are considered in the present work. Thus, the rises of the chords f_b and f_r, as well as $f_{0,b}$ and $f_{0,r}$, must obey the following condition:

$$\frac{L}{f} \geq \varsigma, \tag{2}$$

where ς is the limiting span-to-rise ratio for the chords, which is taken the following: $\varsigma = 8$.

The bearer chord of the roof structure is a steel cable or a cable bundle with the overall axial stiffness EA_b. The restraining chord is composed of a cable '*cab*' with the stiffness $EA_{r,cab}$ and a membrane shell '*m*'. In the present work, the shell is modeled by means of membrane-simulating element, which behaves under load like an ordinary cable with the stiffness $\overline{EA}_{r,m}$.

Considering the equality of the relative deformations $\left(\varepsilon_r = \varepsilon_{r,cab} = \varepsilon_{r,m}\right)$, the overall stiffness EA_r of the restraining chord is the sum of the stiffness values of its components:

$$EA_r = EA_{r,cab} + \overline{EA}_{r,m}. \tag{3}$$

The axial force N in a chord or its components is obtained by Hook's law:

$$N = EA \cdot \varepsilon, \tag{4}$$

where EA is the axial stiffness; ε is the chord's relative elongation given the rise f:

$$\varepsilon = \frac{L_c}{L_{c0}} - 1, \tag{5}$$

where L_c and L_{c0} are the current and initial chord lengths, respectively:

$$L_c = \Psi_4 \cdot f^4 + \Psi_2 \cdot f^2 + L; \tag{6}$$

$$L_{c0} = L_g - \Delta L_p, \tag{7}$$

where $\Psi_2 = 8/\left(3 \cdot L\right)$ and $\Psi_4 = -32/\left(5 \cdot L^3\right)$ are the coefficients for a parabola-shaped curve; L_g is the geometric length of the chord, obtained from (6) given the initial rise f_0; ΔL_p is the tensioning of the chord, which is introduced for pre-stressing the roof structure.

The effective stiffness of the membrane-simulating element $\overline{EA}_{r,m}$ is proposed to be obtained numerically. The membrane is substituted by a mesh of elastic elements. The initial shape of the mesh is obtained by means of the force density method [30, 31]. The membrane is loaded along the ridge with uniformly distributed test load q (Fig. 4). An auxiliary cable with the stiffness $EA_{r,cab}^{aux}$ is used for redistributing the load and transmitting it to the membrane. Finite element method is used for the analysis.

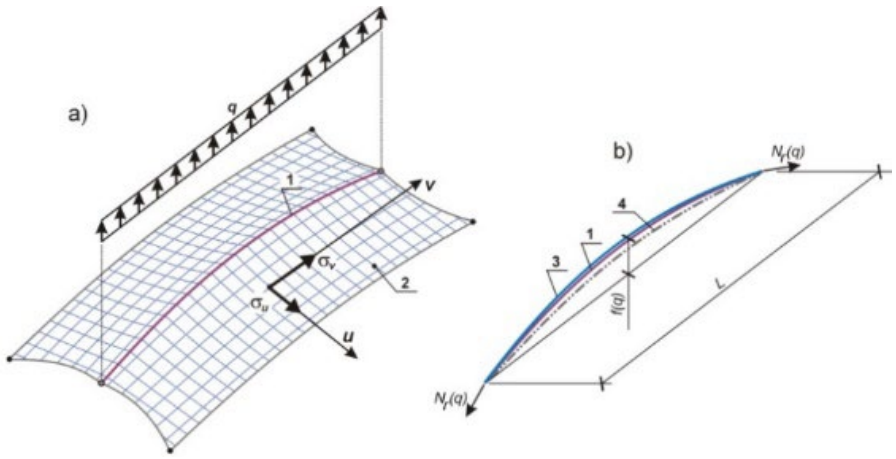

Figure 4. Determination of the effective stiffness of the membrane-simulating element $\overline{EA}_{r,m}$: a – the model for the finite element analysis; b – structural model for the stiffness calculation; 1 – the auxiliary cable with the stiffness $EA_{r,cab}^{aux}$; 2 – the membrane; 3 – the membrane-simulating element; 4 – the initial shape of the ridge of the membrane; σ_u and σ_v are the membrane stresses in the principal directions *u* and *v*.

The membrane with the auxiliary cable deforms from the initial rise $f_{0,r}$ to the resultant one. The effective stiffness $\overline{EA}_{r,m}$ is calculated by the following expression:

$$\overline{EA}_{r,m} = \frac{N_r(q)}{\varepsilon_r\left(f(q)\right)} - EA_{r,cab}^{aux}, \tag{8}$$

where $N_r(q) = \frac{q \cdot L^2}{8 \cdot f(q)}$ is the overall axial force in the restraining chord; $f(q)$ is the rise of the chord under the load q; $\varepsilon_r\left(f(q)\right)$ is the relative elongation of the chord (5) given the rise $f(q)$ and the chord tensioning $\Delta L_p = 0.$

The girder equilibrates the horizontal forces, which are induced by the cable truss. Considering, that the membrane effective force is distributed by the catenary cables between the girder and the neighboring fixed supports (Fig. 2), the axial force in the girder N_{grd} is estimated as follows:

$$N_{grd} = N_{b,cab} + N_{r,cab} + \frac{N_{r,m}}{2}, \tag{9}$$

where $N_{b,cab}$ and $N_{r,cab}$ are the forces in the bearer chord and in the cable of the restraining chord, respectively; $N_{r,m}$ is the membrane effective force.

The axial force in the girder, being compressible, is taken positive in the present work. The ultimate limit state condition for the girder may be written as follows:

$$\Theta_{grd} \le \Theta_{\lim,grd}, \tag{10}$$

where $\Theta_{\lim,grd}$ is the allowable stress-strength ratio for the girder; Θ_{grd} is the ratio given the axial force N_{grd} and the maximum absolute value of the bending moment M_{grd}:

$$\Theta_{grd} = \frac{N_{grd}}{\varphi_e \cdot A_{grd} \cdot R_{grd}}, \text{ if } m_{ef} < 20; \tag{11}$$

$$\Theta_{grd} = \frac{M_{grd}}{W_{grd} \cdot R_{grd}}, \text{ otherwise,} \tag{12}$$

where A_{grd} and W_{grd} are the area and the elastic section modulus of the girder's cross section; R_{grd} is the material strength of the girder; φ_e is the buckling coefficient which is obtained by the Design Code (SP 16.13330.2017) given the effective slenderness $\overline{\lambda}$ and the adjusted relative eccentricity m_{ef}.

Bending moment in the girder M_{grd} is induced by transverse and longitudinal impacts:

$$M_{grd} = M_Q + N_{grd} \cdot \delta, \tag{13}$$

where M_Q is the bending moment brought about by the transverse load; δ is the deflection of the girder under load:

$$\delta = \frac{\delta_Q}{1 - N_{grd} / N_{el}}, \tag{14}$$

where δ_Q is the deflection by the transverse load only; N_{el} is the Euler load, $N_{grd} < N_{el}$:

$$N_{el} = \pi^2 \cdot E_{grd} \cdot I_{grd} / L^2. \tag{15}$$

Considering the chords of the cable structure, the limit state conditions may be written as follows:

– the ultimate limit state:

$$\Theta_c \le \Theta_{\lim,2}; \tag{16}$$

– the serviceability limit state:

$$\omega_{ld} \le \omega_{\lim}; \tag{17}$$

$$\Theta_{\lim,1} \le \Theta_c, \tag{18}$$

where ω_{ld} is the deflection caused by the external load; $\omega_{\lim}$ is the allowable deflection; Θ_c is the stress-strength ratio for the chord, while $\Theta_{\lim,1}$, $\Theta_{\lim,2}$ are the allowable boundary values:

$$\Theta_c = \frac{\sigma_c}{R_c} \in \left[\Theta_{\lim,1} \ldots \Theta_{\lim,2}\right], \tag{19}$$

where σ_c is the normal stress in the chord; R_c is the chord's strength.

Having considered Hook's law, the ratio Θ_c can be converted as follows:

$$\Theta_c = \varepsilon / \zeta, \tag{20}$$

where ζ is the maximum relative deformation given the material strength and the stiffness properties.

Considering the cable elements of the chords, the ζ_{cab}-value is obtained as follows:

$$\zeta_{cab} = R_{cab} / E_{cab}, \tag{21}$$

where R_{cab} and E_{cab} are the strength and the modulus of elasticity of the steel cables.

The allowable deformation of the bearer cable can be written as follows:

$$\varepsilon_b \in \left[\varepsilon_{cab,1} \ldots \varepsilon_{cab,2}\right], \tag{22}$$

where

$$\varepsilon_{cab,1} = \Theta_{\lim,1} \cdot \zeta_{cab}; \tag{23a}$$

$$\varepsilon_{cab,2} = \Theta_{\lim,2} \cdot \zeta_{cab}. \tag{23b}$$

Considering the membrane-simulating element of the restraining chord, the ζ_m-value is obtained numerically:

$$\zeta_m = \varepsilon_r \left(f_{m,\lim} \right), \tag{24}$$

where ε_r is the relative elongation (5) given the maximum rise of the restraining chord $f_{m,\lim}$ under the conditions:

$$\sigma_u \le \sigma_{\lim,u}; \tag{25a}$$

$$\sigma_v \le \sigma_{\lim,v}, \tag{25b}$$

where σ_u and σ_v are the membrane stresses in the u and v directions (Fig. 4); $\sigma_{\lim,u}$ and $\sigma_{\lim,v}$ are the allowable membrane stresses in the orthotropic shell:

$$\sigma_{\lim} = \sigma_{break} / K, \tag{26}$$

where σ_{break} is the membrane breaking strength; K is the stress factor [42].

The allowable range for the relative deformations of the restraining chord in a whole:

$$\varepsilon_r \in \left[\varepsilon_{r,1} \ldots \varepsilon_{r,2} \right], \tag{27}$$

where $\varepsilon_{r,1}$ and $\varepsilon_{r,2}$ are the following boundary values:

$$\varepsilon_{r,1} = \max \left(\varepsilon_{cab,1},\ \varepsilon_{m,1} \right); \tag{28a}$$

$$\varepsilon_{r,2} = \max \left(\varepsilon_{cab,2},\ \varepsilon_{m,2} \right), \tag{28b}$$

where $\varepsilon_{cab,i}$ are the limiting deformations of the cable element of the restraining chord (23), while $\varepsilon_{m,i}$ are the limiting deformations of the membrane-simulating element:

$$\varepsilon_{m,i} = \Theta_{\lim,i} \cdot \zeta_m, \tag{29}$$

where $i = \{1, 2\}$, and ζ_m is given by (24).

Pre-stressing of the roof and the operational phase are considered separately. At the pre-stressing phase the roof structure cambers by the distance Δf_{pr} thus transforming the chords' rises from f_0 into f_{pr} (1):

$$\Delta f = \Delta f_{pr}; \tag{30a}$$

$$\Delta f_{1/4} = 0.75 \cdot \Delta f_{pr}. \tag{30b}$$

The cambering of the roof is induced by tensioning of the bearer chord. The girder is subjected by its own weight ρ_{grd} in the vertical direction, while the weight of the cable truss and the membrane is considered negligible. The longitudinal force in the girder N_{grd}^{pr} is brought about by the cables.

At the operational phase, the roof deforms downwards under vertical external loads. The full uniform load Q_{tot}, as well as partial uniform load Q_{prt} and the load Q_{hlf} acting on a half of the span of the roof,

are taken into account (Fig. 5). It is assumed, that the full uniform load exceeds the overall sum of the non-uniform impacts:

$$Q_{prt} + Q_{hlf} \le Q_{tot}. \tag{31}$$

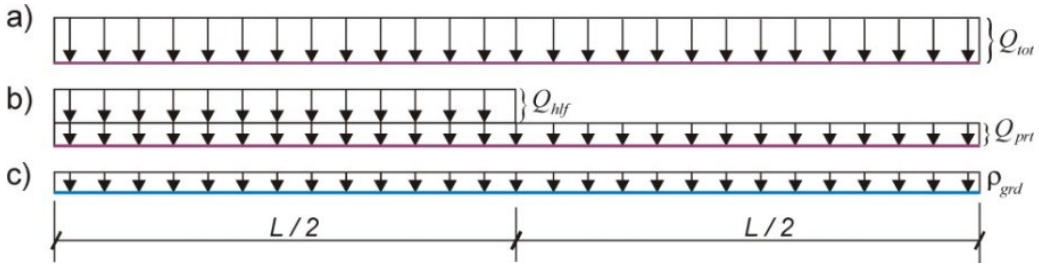

Figure 5. External loads considered: a – the full uniform load, b – non-uniform load, c – the girder's own weight.

Under a uniformly distributed load, the chord's rises transform into f_{ld} (1) by the following overall displacements:

$$\Delta f = \Delta f_{pr} - \omega_{ld}; \tag{32a}$$

$$\Delta f_{1/4} = 0.75 \cdot \left(\Delta f_{pr} - \omega_{ld} \right), \tag{32b}$$

where ω_{ld} is the deflection of the roof at the center of the span.

The deflection of the roof under the full uniform load Q_{tot} is considered equal to the allowable deformation $\omega_{ld} = \omega_{\lim}$. It is assumed, that the cable truss takes the full amount of the load Q_{tot}, and the bearer chord reaches the ultimate limit state: $\varepsilon_{ld,b} = \varepsilon_{cab,2}$. The girder is only influenced by its own weight ρ_{grd} and by the longitudinal forces N_{grd}^{ld}.

The non-uniform load considered in the research consists of a uniform part Q_{prt} and a half-span load Q_{hlf} (Fig. 5). The partial uniform load Q_{prt} is completely taken by the cable truss, while the half-span load splits between the truss and the girder into $Q_{hlf,t}$ and $Q_{hlf,grd}$, respectively:

$$Q_{hlf,t} = \xi_{Qh} \cdot Q_{hlf}; \tag{33a}$$

$$Q_{hlf,grd} = \left(1 - \xi_{Qh}\right) \cdot Q_{hlf}, \tag{33b}$$

where $\xi_{Qh} \in (0 \ldots 1]$ is the parameter of splitting the load, which is to be determined.

Thus, the left-hand side of the cable truss is influenced by the load Q_L, while the load Q_R acts on the right part of the span (Fig. 6):

$$Q_L = Q_{prt} + Q_{hlf,t}; \tag{34a}$$

$$Q_R = Q_{prt}. \tag{34b}$$

The corresponding loads acting on the girder are the following:

$$Q_{L,grd} = \rho_{grd} + Q_{hlf,grd}; \tag{35a}$$

$$Q_{R,grd} = \rho_{grd}. \tag{35b}$$

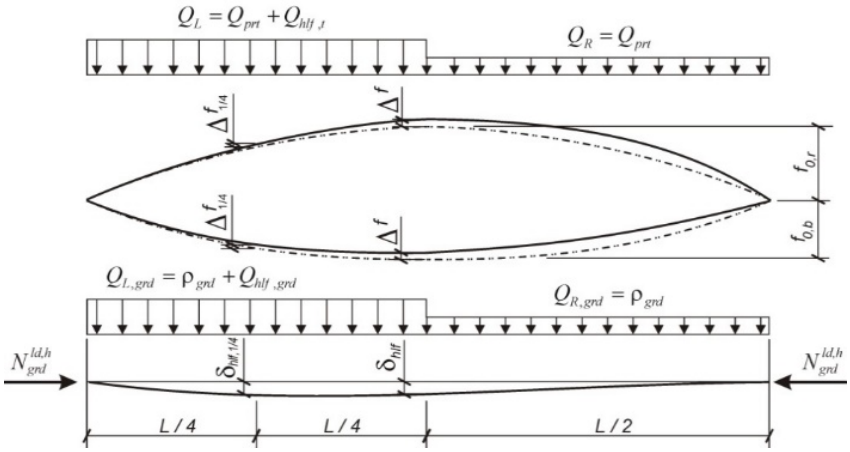

Figure 6. Structural model under the non-uniform load.

The parameter of splitting the load, ξ_{Qh}, is obtained by the condition of compatibility of deformations of the truss and the girder in the quarter of the span. The secant method is used.

The girder deflection $\delta_{1/4}$ is obtained by (14) given the loads $Q_{L,grd}$ and $Q_{R,grd}$. The overall displacements of the cable truss (Δf and $\Delta f_{1/4}$, Fig. 6) under the loads Q_L and Q_R are obtained by minimization of the following discrepancy using the coordinate descent method:

$$\Xi = |\vartheta_1| + |\vartheta_2| \to 0, \tag{36}$$

where the functions $\vartheta_1\left(\Delta f, \Delta f_{1/4}\right)$ and $\vartheta_2\left(\Delta f, \Delta f_{1/4}\right)$ are derived from [43]:

$$\vartheta_1 = \frac{f_{0,b} - \Delta f}{q_{Sym} + p_{Eq}} \cdot \frac{\Delta L_{c,b}}{\rho_b} - 1; \tag{37a}$$

$$\vartheta_2 = \frac{q_{Inv} + \eta_r \cdot p_{Eq}}{q_{Sym} + p_{Eq}} \cdot \frac{1}{\eta_b} - 1, \text{ if } \eta_b \neq 0, \text{ and } \vartheta_2 = 1 \text{ otherwise}, \tag{37b}$$

where p_{Eq} is the link load between the chords and η_b, η_r are the coefficients of load non-uniformity, which depend on the displacements Δf and $\Delta f_{1/4}$; $\Delta L_{c,b}$ is the bearer chord elongation given the η_b-value; ρ_b and ρ_r are the ratios, which depend on the chords stiffness properties; q_{Sym} and q_{Inv} are the symmetrical and inverse-symmetrical parts of the external load:

$$q_{Sym} = \frac{Q_L + Q_R}{2}; \tag{38a}$$

$$q_{Inv} = \frac{Q_L - Q_R}{2}. \tag{38b}$$

The value $\eta_b = 0$ means, that the load must be uniform. It contradicts the assumption, that there is non-zero impact Q_{hlf}, thus raising the maximum discrepancy value in (37b).

The coordinate descent method is used for minimizing the discrepancy (36). Having started from the initial guess values $\left(\Delta f,\ \Delta f_{1/4}\right)_{init} = \left(\Delta f_{pr}/2, 0\right)$ the result is achieved iteratively by variation of the displacements.

3. Results and Discussion

The roof structure, considered in the research, consists of the framework and the flexible membrane shell. The framework is protected by the patent RF no. 2439256, 2010.

3.1. The allowable rise of a parabola-shaped chord

The rise of a parabola-shaped chord at the center of the span f_c is derived given the chord's length L_c:

$$f_c = \frac{L}{2} \cdot \sqrt{\frac{5}{6}} \cdot \sqrt{1 - \sqrt{1 - 3.6 \cdot \left(\frac{L_c}{L} - 1 \right)}}. \quad (39)$$

Considering that the radical expressions in (39) must be positive, the length of the chord is confined as follows:

$$L_c \in [1.0 \ldots 1.278] \cdot L. \quad (40a)$$

On the other hand, substituting the boundary values for the chord rises ($f = 0$ and $f = L/\varsigma$ (2)) into (6) yields in the following range:

$$L_c^{\lim} \in \left[1.0 \ldots \left(\frac{-32}{5 \cdot \varsigma^4} + \frac{8}{3 \cdot \varsigma^2} + 1.0 \right) \right] \cdot L. \quad (40b)$$

Considering $\varsigma = 8,$ one can see, that the range (40b), $L_c^{\lim} \in [1.0 \ldots 1.04] \cdot L,$ fully belongs to (40a), thus providing no singularity in (39).

Assuming, that the chord reaches a limit state, the allowable length $L_c^{\lim}$ is the following:

$$L_c^{\lim} = L_{c0} \cdot (\varepsilon_{\lim} + 1), \quad (41)$$

where $\varepsilon_{\lim}$ is a boundary value $\varepsilon_{cab,i}$ or $\varepsilon_{r,i}$ (22 or 27), $i = \{1, 2\}$; L_{c0} is the initial chord's length (7).

Substituting the length $L_c^{\lim}$ into (39) gives the allowable rise of a parabola-shaped chord under the limit states condition specified.

3.2. Deformation of the roof at the pre-stressing phase

Considering the restraining chord, the deformation of the roof during the pre-stressing Δf_{pr} is confined as follows:

$$\Delta f_{pr} \in [\Delta f_{pr,\lim 1},\ \Delta f_{pr,\lim 2}], \quad (42)$$

where $\Delta f_{pr,\lim 1}$ and $\Delta f_{pr,\lim 2}$ are the following boundary values:

$$\Delta f_{pr,\lim 1} = f_{\lim_1,r} + \omega_{\lim} - f_{0,r}; \quad (43a)$$

$$\Delta f_{pr,\lim 2} = f_{\lim_2,r} - f_{0,r}, \quad (43b)$$

where $f_{\lim_1,r},\ f_{\lim_2,r}$ are the lower and upper bounds for the rise of the restraining chord, respectively.

The $f_{\lim_1,r}$-value is calculated by (39) given the allowable length (41) $L_{c,r}^{\lim 1} = L_{c0,r} \cdot (\varepsilon_{r,1} + 1)$, while the $f_{\lim_2,r}$-value is obtained as follows:

$$f_{\lim_2,r} = \min\left(f_{\lim 2,r}^{u},\ f_{\lim 2,r}^{s} \right), \quad (44)$$

where $f^{s}_{\lim 2,r} = L/\varsigma$ is imposed by the condition of the shallow shape of the chord (2), while $f^{u}_{\lim 2,r}$ is obtained by (39) given the length, which is determined by the ultimate limit state condition $L^{\lim}_{c,r}2 = L_{c0,r} \cdot \left(\varepsilon_{r,2} + 1\right)$; $L_{c0,r}$ is obtained by (7) for the restraining chord given $\Delta L_p = 0$.

In order to keep the range (42) nonsingular the allowable deflection $\omega_{\lim}$ must obey the following condition:

$$\omega_{\lim} \le \omega_{\lim,up} = f_{\lim_2 r} - f_{\lim_1 r}. \tag{45a}$$

The serviceability limit state also confines the $\omega_{\lim}$ -range:

$$\omega_{\lim} \le \Omega_{\lim}, \tag{45b}$$

where $\Omega_{\lim}$ is the given value, which is defined for preventing large structural deformations.

Considering the bearer chord, the serviceability limit state imposes the following condition on its rise:

$$f_{pr,b} \ge f_{\lim 1,b}, \tag{46}$$

where $f_{pr,b}$ is the chord's rise (1a) given the roof deformation at the phase of the pre-stressing (30a); $f_{\lim 1,b}$ is obtained by (39) given the allowable chord's length $L^{\lim}_{c,b}1 = L_{c0,b} \cdot \left(\varepsilon_{cab,1} + 1\right)$; $L_{c0,b}$ is the initial length of the bearer chord, derived from the ultimate limit state condition:

$$L_{c0,b} = L^{ld}_{c,b} \cdot \frac{1}{1 + \varepsilon_{cab,2}}, \tag{47}$$

where $L^{ld}_{c,b}$ is the length (6) of the bearer cable given the rise $f_{ld,b}$ (1a), which corresponds to the displacement (32a).

Both sides of (46) depend on the deformation of the roof at the phase of the pre-stressing, Δf_{pr}. Thus, it supplements the condition (42) imposed on the Δf_{pr} -range.

3.3. The stiffness of the chords

Considering Hook's law and the uniformity of the load distribution at the pre-stressing phase, the axial stiffness values of the chords EA_b and EA_r may be written as follows:

$$EA_b = P_{pr} \cdot \frac{L^2}{8 \cdot f_{pr,b} \cdot \varepsilon_{pr,b}}; \tag{48a}$$

$$EA_r = P_{pr} \cdot \frac{L^2}{8 \cdot f_{pr,r} \cdot \varepsilon_{pr,r}}, \tag{48b}$$

where the chord rises $f_{pr,b}$, $f_{pr,r}$ and the corresponding relative deformations $\varepsilon_{pr,b}$, $\varepsilon_{pr,r}$ are determined by the roof's cambering Δf_{pr}; P_{pr} is the link load between the chords at the pre-stressing phase.

The boundary value for the link load between the chords is obtained under the condition that the full uniform load Q_{tot} is completely taken by the cable truss:

$$P_{pr,bound} = \frac{Q_{tot}}{\frac{f_{ld,b} \cdot \varepsilon_{cab,2}}{f_{pr,b} \cdot \varepsilon_{pr,b}} - \frac{f_{ld,r} \cdot \varepsilon_{ld,r}}{f_{pr,r} \cdot \varepsilon_{pr,r}}}, \quad (49)$$

where $\varepsilon_{cab,2}$ is the limiting deformation (23b), which ensures the full use of the strength properties of the bearer chord under the condition of reaching the allowable rise $f_{ld,b}$ under load; $\varepsilon_{pr,b}$, $\varepsilon_{ld,r}$ and $\varepsilon_{pr,r}$ are the relative deformations of the chords given the rises $f_{pr,b}$, $f_{ld,r}$ and $f_{pr,r}$, respectively.

If the link load is less than its boundary value, $P_{pr} < P_{pr,bound}$, then the cable truss takes only a fraction of the uniform load Q_{tot}. The remaining part of Q_{tot} influences the girder and increases its material capacity. If the link load exceeds the boundary value $P_{pr} > P_{pr,bound}$, then the structure deforms less, than it is allowed by the serviceability limit state: $\omega_{ld} < \omega_{\lim}$. Both cases are worse from the economic point of view, than the case of $P_{pr} > P_{pr,bound}$, when the deformation is equal to the allowable one and the cable truss, being subjected by uniform loads, induces only horizontal force in the girder.

3.4. The design clearances

The design clearances are used in emergency-proof girders in form of “curved gains” thus using the principle of passive adaptability [21, 22]. They allow transformation of the construction in order to enhance structural performance. The clearances Δ (loose connections, Fig. 1) are introduced into the structural framework of the roof after the pre-stressing phase is completed.

Assuming, that the uniform load Q_{tot} is fully taken by the cable truss, the design clearance at the center of the span may be expressed as follows:

$$\Delta_{1/2} = \omega_{\lim} + \delta_{pr} - \delta_{ld}, \quad (50)$$

where δ_{pr} and δ_{ld} are the deformations of the girder (14) at the center of the span under its own weight ρ_{grd} and the horizontal loads N_{grd}^{pr} and N_{grd}^{ld}, respectively.

The expressions for the horizontal loads, which are brought about by the cable chords, may be written according to (4) and (9) as follows:

$$N_{grd}^{pr} = N_{b,cab}^{pr} + N_{r,cab}^{pr} + \frac{N_{r,m}^{pr}}{2}; \quad (51a)$$

$$N_{grd}^{ld} = N_{b,cab}^{ld} + N_{r,cab}^{ld} + \frac{N_{r,m}^{ld}}{2}, \quad (51b)$$

where

$$N_{b,cab}^{pr} = EA_b \cdot \varepsilon_{pr,b},\ N_{r,cab}^{pr} = EA_{r,cab} \cdot \varepsilon_{pr,r},\ N_{r,m}^{pr} = \overline{EA}_{r,m} \cdot \varepsilon_{pr,r}; \quad (51c)$$

$$N_{b,cab}^{ld} = EA_b \cdot \varepsilon_{cab,2},\ N_{r,cab}^{ld} = EA_{r,cab} \cdot \varepsilon_{ld,r},\ N_{r,m}^{ld} = \overline{EA}_{r,m} \cdot \varepsilon_{ld,r}, \quad (51d)$$

The design clearance at the quarter point of the span may be written in a similar way:

$$\Delta_{1/4} = 0.75 \cdot \omega_{\lim} + \delta_{pr,1/4} - \delta_{ld,1/4}, \quad (52)$$

where $\delta_{pr,1/4}$ and $\delta_{ld,1/4}$ are the girder’s deformations at the quarter point of the span under the loads ρ_{grd}, N_{grd}^{pr} and N_{grd}^{ld}.

Considering the uniformity of the load Q_{tot}, the design clearance values throughout the span are taken by the parabola-shaped curve.

3.5. Non-uniform load on the roof

The non-uniform load considered in the research is shown in Figs. 5 and 6. In order to split the load Q_{hlf} between the truss and the girder by ξ_{Qh}-parameter (33) the condition of compatibility of deformations at the quarter point of the span may be written as follows:

$$\omega_{h,1/4} = \Delta_{1/4} + \delta_{h,1/4} - \delta_{pr,1/4}, \tag{53}$$

where $\omega_{h,1/4}$ and $\delta_{h,1/4}$ are the deformations of the truss and the girder under the loads $\left(Q_L,\ Q_R\right)$ and $\left(Q_{L,grd},\ Q_{R,grd}\right)$, respectively; $\delta_{pr,1/4}$ is the deformation of the girder under its own weight at the pre-stressing phase.

Substituting (52) into (53) yields in the following equation in one unknown ξ_{Qh}:

$$h\left(\xi_{Qh}\right) = 0, \tag{54a}$$

where $h\left(\xi_{Qh}\right)$ is the following function:

$$h\left(\xi_{Qh}\right) = \frac{0.75 \cdot \Delta f_{pr} + \delta_{ld,1/4} - \Delta f_{1/4}}{0.75 \cdot \omega_{\lim} + \delta_{h,1/4}} - 1, \tag{54b}$$

where $\Delta f_{1/4}$ is the overall displacement of the cable truss at the quarter point of the span, which includes the displacement at the pre-stressing phase and the displacement under the non-uniform load $\left(Q_L,\ Q_R\right)$:

$$\Delta f_{1/4} = 0.75 \cdot \Delta f_{pr} - \omega_{h,1/4}. \tag{54c}$$

Only $\Delta f_{1/4}$ and $\delta_{h,1/4}$-values in (54b) depend on ξ_{Qh}, while all the remaining terms may be held constant. The value $\delta_{h,1/4}$ is obtained from (14), while $\Delta f_{1/4}$-value is obtained by the minimization of (36) given the ξ_{Qh}-ratio.

The value of ξ_{Qh}, which closely satisfies (54a), is obtained by means of the iterative secant method. The middle point ξ_M between the left and right bounds (ξ_L and ξ_R) is obtained as follows:

$$\xi_M = \frac{\left|h\left(\xi_R\right)\right| \cdot \xi_L + \left|h\left(\xi_L\right)\right| \cdot \xi_R}{\left|h\left(\xi_R\right)\right| + \left|h\left(\xi_L\right)\right|}, \tag{55a}$$

under the condition:

$$h\left(\xi_R\right) > 0. \tag{55b}$$

The bounds, used by ξ_L = 0.0 and ξ_R = 1.0, are modified during the iteration process as follows: if $h\left(\xi_R\right) \cdot h\left(\xi_M\right) > 0$, then $\xi_R = \xi_M$ and $\xi_L = \xi_M$, otherwise. Having reached the acceptable value of the discrepancy μ_ε $\left(\left|h\left(\xi_M\right)\right| < \mu_\varepsilon\right)$, the iteration process finishes: $\xi_{Qh} = \xi_M$.

If, however, the condition (55b) is not met, the girder does not take transverse load $\left(\xi_{Qh} = 1.0\right)$ and the deformations of the cable truss are less than the design clearances.

3.6. Numerical example

3.6.1. General specification

A fragment of the roof structure is considered as an example. The fragment is highlighted in blue in Fig. 2. It consists of the cable truss with the girder and two pieces of the membrane. The membrane is situated symmetrically about the ridge of the truss.

The span of the roof L is 12 m. The initial chords' rises are taken the following: $f_{0,b}$ = 1.5 m and $f_{0,r}$ = 1.0 m. The rise-to-span ratio for the bearer chord $\left(f_{0,b}/L = 1/8\right)$ belongs to the optimal range $\left[1/10 \ldots 1/6\right]$ providing efficient force transfer to the supporting structures [44]. The rise-to-span ratio for the restraining chord $\left(f_{0,r}/L = 1/12\right)$ belongs to the allowable range $\left[1/20 \ldots 1/10\right]$ in order to reduce the overall height of the roof [33]. The width of the fragment B is 6 m. The following loads are considered: Q_{tot} = 18 kN/m, Q_{prt} = 9.0 kN/m and Q_{hlf} = 9.0 kN/m (Fig. 5). The allowable displacement of the roof under load is $\Omega_{\lim}$ = 0.1 m.

The girder is made of two steel channel bars with the following strength property and the modulus of elasticity: R_{grd} = 2.1·10^5 kN/m^2 and E_{grd} = 2.1·10^8 kN/m^2. The allowable stress-strength ratio is adopted the following: $\Theta_{\lim,grd}$ = 1.0.

The chords of the truss are made of steel cables with the following material properties: R_{cab} = 7.0·10^5 kN/m^2 and E_{cab} = 1.3·10^8 kN/m^2. Thus, the maximum relative deformation of the cables is ζ_{cab} = 5.385·10^{-3} (21). The boundary values for the stress-strength ratio of the chords are taken the following: $\Theta_{\lim,1}$ = 0.01 and $\Theta_{\lim,2}$ = 1.0.

The membrane is made of architectural fabrics with the elastic moduli E_u = 600 kN/m and E_v = 400 kN/m in u and v-directions, respectively. The membrane axes are shown in Fig. 4. They coincide with the direction of the main curvatures [44].

Considering the stress factor K = 5.0 [42, 45], the allowable membrane stresses are the following: $\sigma_{\lim,u}$ = 15 kN/m and $\sigma_{\lim,v}$ = 12 kN/m. The membrane pre-tension is taken 1.5 kN/m in u and v-directions that complies with the requirements [42].

3.6.2. Obtaining the effective stiffness and the allowable relative deformation of the membrane-simulating element

The membrane is numerically simulated using the specialized software package for nonlinear structural analysis EASY [46]. The membrane is substituted by a mesh of the size 0.5 m, which belongs to the range $[0.1...0.6]$ m considered in [47]. An auxiliary cable is used for redistributing the test load q along the membrane ridge (Fig. 4). The membrane is able to slide along the auxiliary, catenary and backstay cables, which are arranged at the perimeter [35]. In order to obtain precise properties of the membrane-simulating element the stiffness of the auxiliary cable must be in the range of the restraining chord stiffness EA_r.

The initial guess for the stiffness of the restraining chord ($EA_{r,guess}$ = 6310 kN) is obtained by (48b) using the $P_{pr,bound}$-value (49), the upper bound for the roof cambering during the pre-stressing $\Delta f_{pr,\lim 2}$ (43b), and the allowable cable deformation $\varepsilon_{cab,2}$ for the restraining chord. Thus, two variants of the auxiliary cable, which do not exceed the $EA_{r,guess}$-value, are taken into account: the cable with the diameter of 6.1 mm ($EA_{r,cab}^{aux,I}$ = 2860 kN) and the cable with the diameter of 8.1 mm ($EA_{r,cab}^{aux,II}$ = 4940 kN) [48].

In both cases the ridge load q (Fig. 4) increases from zero up to the value $q_{\lim}$, which results in

failing one of the conditions (25). The increment of the load q is 3.0 kN/m. The maximum loads are $q_{\lim,I}$ = 24 kN/m and $q_{\lim,II}$ = 30 kN/m for the cases considered. The peak stresses in the membrane in u and v directions, as well as the rise of the auxiliary cables in the middle of the span $f(q)$ given the load q are obtained by the EASY-software. The membrane stresses are shown in Fig. 7.

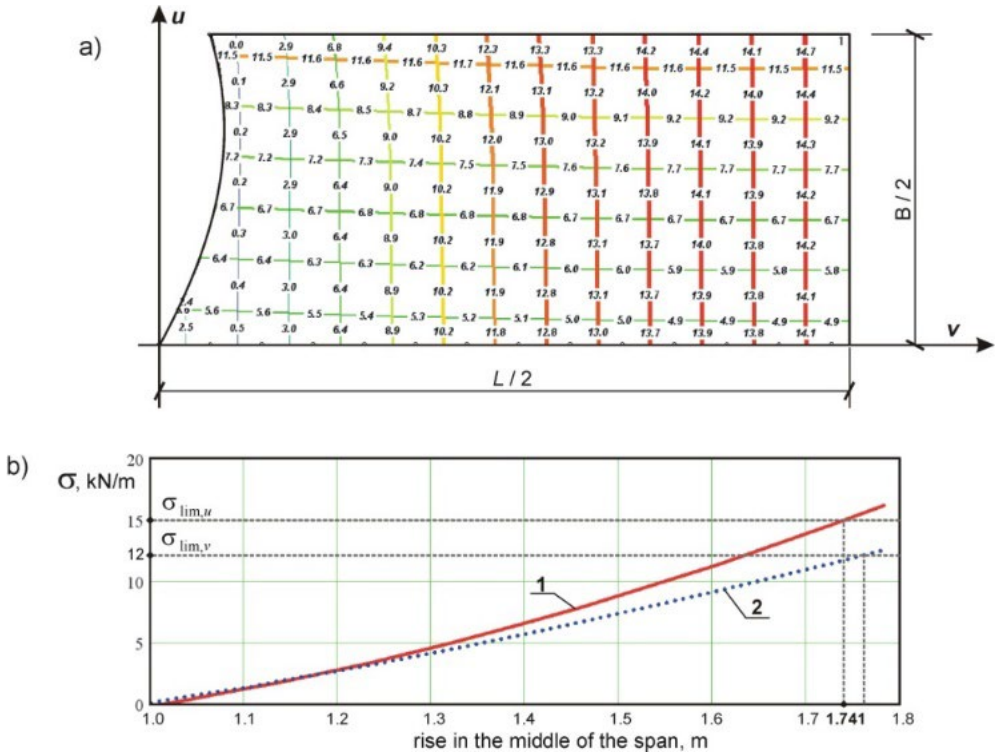

Figure 7. The membrane stresses induced by the increase of the rise in the middle of the ridge: a – the membrane stress distribution, kN/m; b – the peak membrane stresses; 1 – the membrane stress in the *u*-direction, σ_u; 2 – the membrane stress in the *v*-direction, σ_v.

The figure shows, that the rise $f_{m,\lim}$, which equals 1.741 m, corresponds to the membrane allowable stress $\sigma_{\lim,u}$. The maximum relative deformation of the membrane-simulating element is obtained by (24) given $f_{m,\lim}$: ζ_m = 0.034. Thus, the allowable range for the relative deformations of the restraining chord (27) is the following: $\varepsilon_r \in \left[3.4 \cdot 10^{-4} \ldots 5.385 \cdot 10^{-3}\right]$.

The graphs of the effective stiffness values $\overline{EA}_{r,m}$ of the membrane-simulating element (8), obtained for the considered variants of the auxiliary cable, are shown in Fig. 8. In spite of substantial nonlinearity of the graphs in the full range of the allowable membrane rise $f_{m,\lim}$ (Fig. 8a), the graphs tend to straight lines and exhibit the variation less than 2 % in the allowable range of the roof structure in the whole (Fig. 8b). This range is determined by the upper bound of the roof cambering during the pre-stressing (43b): $\Delta f_{pr,\lim 2}$ = 0.143 m. Thus, the averaged effective stiffness value may be applied: $\overline{EA}_{r,m}$ = 3560 kN.

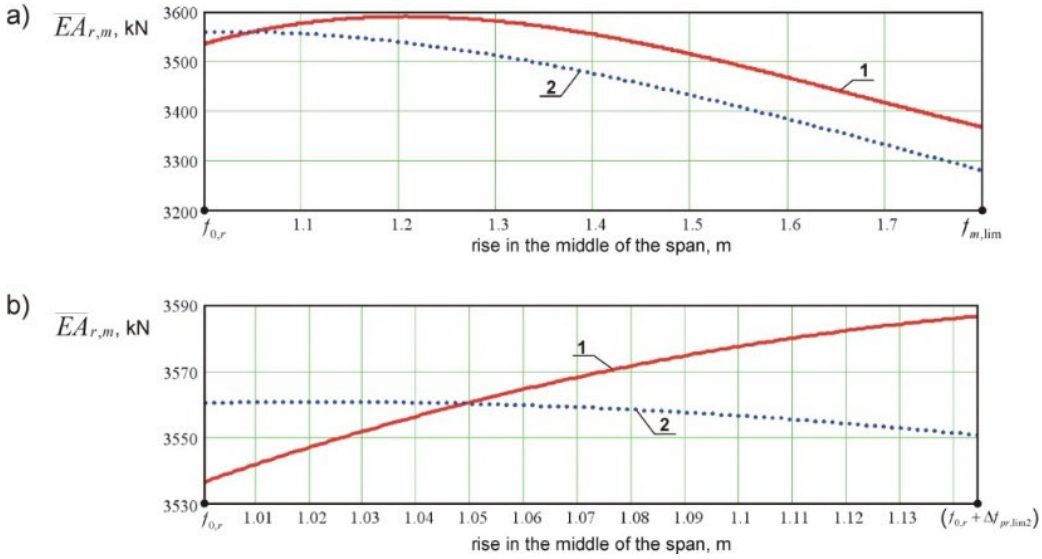

Figure 8. The graphs of the effective stiffness values $\overline{EA}_{r,m}$ of the membrane-simulating element: a – the full range of the allowable membrane rise, b – the allowable range for the rise of the restraining chord as a composite element; 1, 2 – curves, which correspond to the first and the second variants of the auxiliary cable, respectively.

3.6.3. Estimating the structural parameters of the roof

The range for the roof deformation at the phase of the pre-stressing Δf_{pr} is determined by (42) and (46). The condition (46) is converted as follows:

$$\chi\left(\Delta f_{pr},\ \omega_{\lim}\right) \geq 0, \tag{56a}$$

where χ is the following function:

$$\chi\left(\Delta f_{pr},\ \omega_{\lim}\right) = \left(f_{pr,b} / f_{\lim 1,b} - 1\right) \cdot 100\%. \tag{56b}$$

The function χ is shown in Fig. 9 for the following cases of the allowable deflection: $\omega_{\lim}$ = {0.08, 0.10, 0.12, 0.133} m. Only those graphs (or their parts), which are situated above the zero-value, ensure the minimum allowed stress in the bearer chord. The green points in the graphs denote the boundary values for the deformation (43a) above which the restraining chord of the roof does not slack under load. The red points denote the upper bound for the deformation (43b) below which the ultimate limit state requirements are fulfilled for the restraining chord.

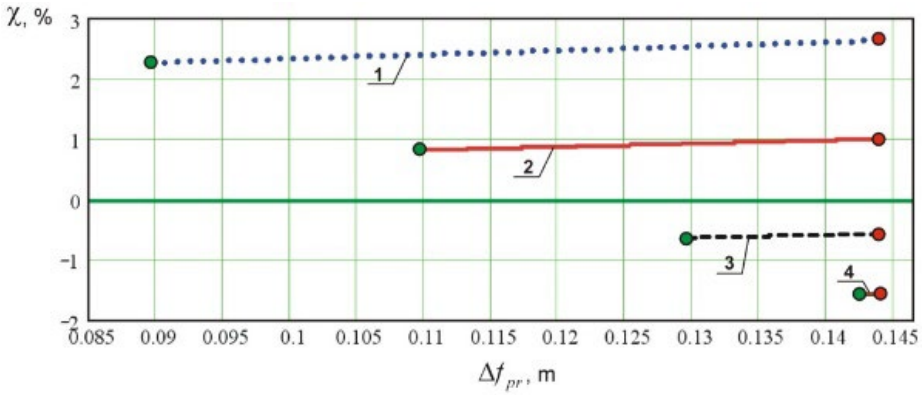

Figure 9. Graphs of χ-function (56b) given the allowable deflections: 1 – ω_{lim}=0.08, 2 – ω_{lim}=0.1, 3 – ω_{lim}=0.12, 4 – ω_{lim}=0.133 m.

The figure shows, that in accordance with growth of the deflection $\omega_{\lim}$, the allowable range for Δf_{pr} decreases. It completely vanishes, when the deflection reaches its upper bound value (45a): $\omega_{\lim,up}$ = 0.134 m.

Considering that the given displacement of the roof meets the condition $\Omega_{\lim} < \omega_{\lim,up}$, it is taken as the allowable deflection: $\omega_{\lim}$ = $\Omega_{\lim}$ = 0.1 m. The corresponding range for the roof cambering is $\Delta f_{pr} \in [0.1096,\ 0.143]$ m. The ratios of the relative deformations of the chords are shown in Fig. 10.

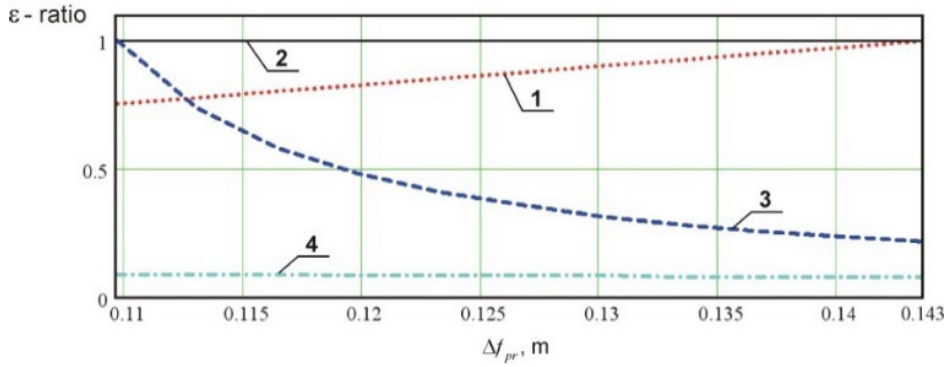

Figure 10. Graphs of ε-ratios: 1 – $\varepsilon_{pr,r} / \varepsilon_{r,2}$; 2 – $\varepsilon_{ld,b} / \varepsilon_{cab,2}$; 3 – $\varepsilon_{r,1} / \varepsilon_{ld,r}$; 4 – $\varepsilon_{cab,1} / \varepsilon_{pr,b}$.

The first two graphs illustrate the ultimate limit state conditions, while graphs 3 and 4 show the serviceability limit state. All the ratios in Fig. 10 are less than or equal to 1.0 meaning that the conditions (22, 27) are met entirely.

Fig. 10 shows that the strength properties of the bearer chord are fully used for all the range of the pre-stressing cambering: $\varepsilon_{ld,b} = \varepsilon_{cab,2}$. The right-hand side bound of the range also provides the full use of the strength properties of the restraining chord $\varepsilon_{pr,r} = \varepsilon_{r,2}$, while at the left-hand side bound the restraining chord keeps the minimum specified tensioning thus remaining workable, $\varepsilon_{ld,r} = \varepsilon_{r,1}$.

The stiffness properties of the chords of the roof are calculated by (48). The restraining chord is a composite element with the overall stiffness equal to the sum of its components [49]. Thus, the stiffness of the restraining cable $EA_{r,cab}$ is obtained from (3) given the stiffness of the membrane-simulating element $\overline{EA}_{r,m}$ and the stiffness of the chord in the whole EA_r. The cross section areas of the cable elements are calculated given the modulus of elasticity E_{cab}.

The graph of the total mass of the cable elements is shown in Fig. 11. The figure shows the trend of the mass increase. The mass growth, however, does not exceed 2.2 %. Cross section areas of the cable chords are shown for the boundary points.

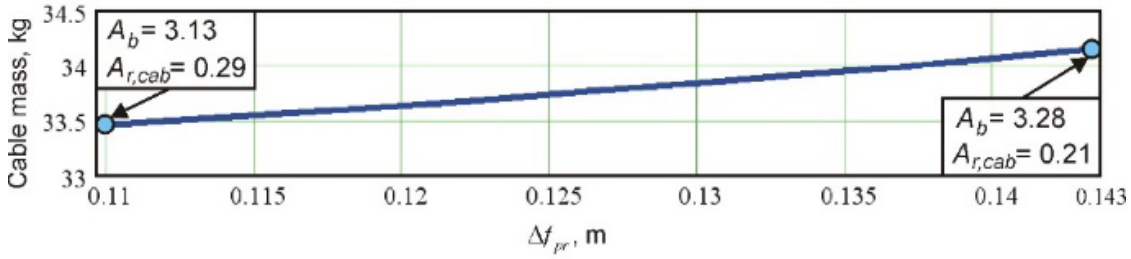

Figure 11. Graph of the total mass of the cable elements, kg (cross section areas of the chords are indicated in cm²).

Considering the girder made of two channel bars, the stress-strength ratios (11, 12) are shown in Fig. 12 for the two load cases: uniform and non-uniform impacts on the roof (Fig. 5). The figure shows, that the half-span load results in higher stress level in the girder, than the full uniform load.

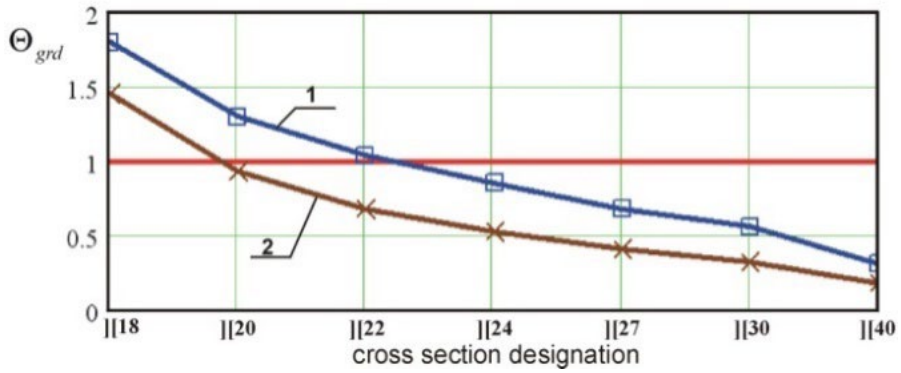

Figure 12. Girder's stress-strength ratios, Θ_{grd}: 1 – partial uniform load Q_{prt} with the half-span load Q_{hlf}; 2 – the full uniform load Q_{tot}.

The graph of structural deformation at the quarter of the span $\omega_{h,1/4}$ brought about by the non-uniform load is shown in Fig. 13. The $\omega_{h,1/4}$ -value is derived from the expression (54c). It is the difference between the roof cambering at the pre-stressing phase and the overall displacement of the cable truss under the load: $\omega_{h,1/4} = 0.75 \cdot \Delta f_{pr} - \Delta f_{1/4}$. Figs. 12 and 13 show, that the channel bars [27 meet all the conditions implied by the ultimate and serviceability limit states.

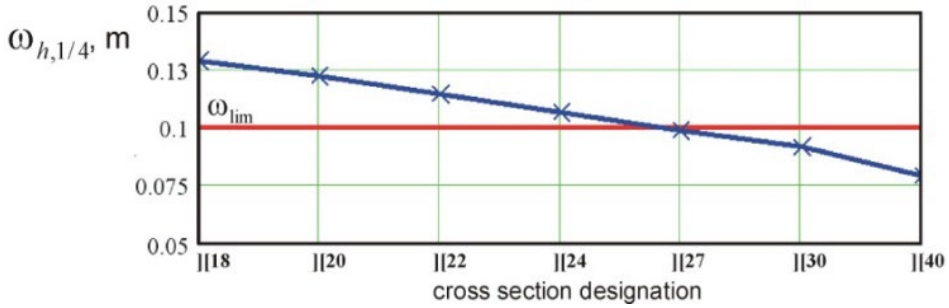

Figure 13. Structural deformation at the quarter of the span induced by the non-uniform load (shown in Fig. 5).

The parameter ξ_{Qh} of splitting the non-uniform load between the cable truss and the girder (33) is shown in Fig. 14. The graph is a hyperbolic-shaped curve, which tends to the asymptote with the increasing of the girder's stiffness.

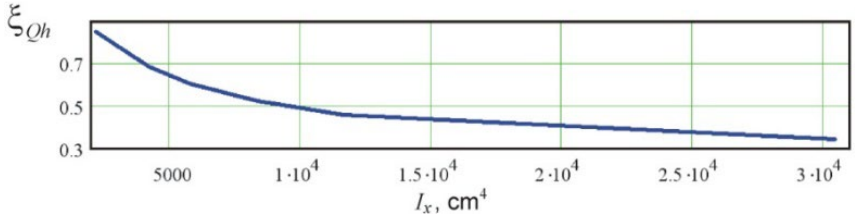

Figure 14. Dependence of the parameter of splitting the load ξ_{Qh} (33) on the moment of inertia of the girder's cross section I_x.

The graph of $h\left(\xi_{Qh}\right)$-ratio (54b) for the girder's cross section chosen (two channel bars [27) is shown in Fig. 15.

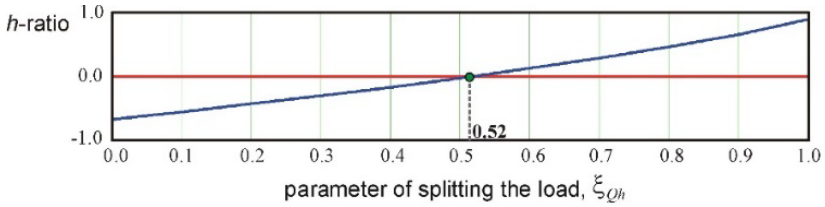

Figure 15. The graph of *h*-ratio (54b).

The figure shows, that the dependence $h\left(\xi_{Qh}\right)$ is close to the linear one in the allowable range $\xi_{Qh} \in (0 \ldots 1]$. Thus, the secant method provides the solution for the equation (54a) in a few iterations. The solution is denoted in the figure by the green point.

3.7. Verification of the results

3.7.1. Comparison with numerical results by the specialized software package

The fragment of the roof, considered in clause 3.6, is numerically simulated using the specialized software package for nonlinear structural analysis EASY.2020 [46] (license no. 15129). The structural model of the roof's fragment is shown in Fig. 16.

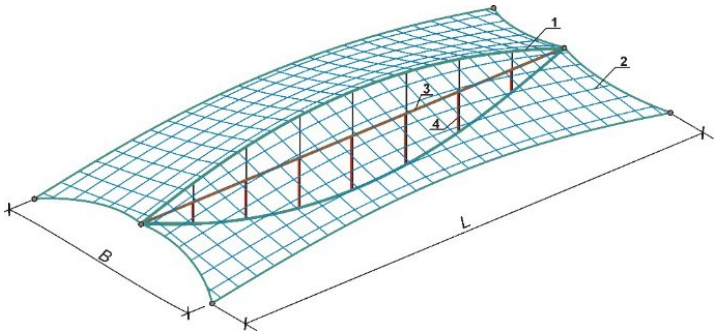

Figure 16. Structural model of the roof's fragment: 1 – cable truss; 2 – flexible membrane; 3 – stiffening girder; 4 – ties for simulating the loose connection (design clearance).

The bearer and restraining chords of the roof are adopted of 24.1 mm and 6.1 mm steel cables, respectively [48]. Corresponding cross section areas of the cables are the following: A_b = 3.38 cm^2 and $A_{r,cab}$ = 0.22 cm^2. They are taken close to the right bound indicated in Fig. 11. Thus, the cambering of the roof is the following: Δf_{pr} = 0.143 m. The tensioning of the bearer chord during the pre-stressing is obtained from (7) given the geometric length $L_{g,b}$ and the initial chord's length $L_{c0,b}$ (47): ΔL_p = 0.093 m. The stiffening girder is adopted of two steel channel bars [27. The geometrical properties of the overall cross section are the following: A_{grd} = 7.04·10^{-3} m^2, W_{grd} = 6.16·10^{-4} m^3 and I_{grd} = 8.32·10^{-5} m^4.

The girder and the roof's framework are not directly connected, unless the supporting points. They are also linked together by vertical ties made of steel cables (elements 4 in Fig. 16). In order to simulate the loose connection, the ties are initially slackened by the design clearance values: $\Delta_{1/2}$ = 0.098 m and $\Delta_{1/4}$ = 0.074 m (50, 52).

Comparison of the main structural parameters, obtained by the proposed expressions, and the results of the numerical analysis by the specialized software package EASY.2020 is given in Table 1.

Table 1. Comparison with the numerical results by the software package EASY.2020.

Designation	Unit	Value		Deviation, ξ, %	Remark
		by the present work	numerically simulated by the EASY-software		
Δf_{pr}	m	0.143	0.139	2.8	(43b)
ω_{ld}	m	0.100	0.101	1.0	must be equal to $\omega_{\lim} = 0.1\,\text{m}$
$\omega_{h,1/4}$	m	0.104	0.098	5.9	(53)
P_{pr}	kN/m	2.16	2.07	4.2	(49)
$N^{pr}{}_{grd}$	kN	52.9	48.3	9.1	(51a)
$N^{ld}{}_{grd}$	kN	236.6	234.9	0.7	(51b)

The table shows good agreement of the results. The peak discrepancy (9.1 %) is at the stage of the pre-stressing, when the axial force in the girder is substantially smaller, than under the external load.

3.7.2. Comparison with the results by the other authors

In order to verify the proposed results the following comparison is implemented. All notations are adopted according to the present paper, except the axial forces in the chords and the horizontal components of the forces, which are denoted by the indexes '*b*' and '*t*' meaning bottom (restraining) and top (bearer) chords.

Consider a symmetric cable truss with the bearer chord arranged above the restraining one [50]. The span of the truss, L, is 60 m. Eight span-to-sag ratios of the chords of the truss are considered: $L/f_{pr,b} = L/f_{pr,r}$ = {7.5, 10.0, 12.5, 15.0, 17.5, 20.0, 22.5, 25.0}. The initial horizontal components of pretension of the chords are the following: $H_{0,b} = H_{0,t}$ = 600 kN. The modulus of elasticity of the cables is E_{cab} = 1.5·10^8 kN/m^2. Cross section areas of the chords are the following: A_b = 2.0·10^{-3} m^2 and A_r = 1.3·10^{-3} m^2. Uniformly distributed load is considered throughout the entire span Q_{tot} = 10.0 kN/m.

Considering the given rises of the chords f_{pr} and the chords' pretensions H_0, the initial lengths of the chords $L_{c,0}$ are obtained by the Hook's law given the chord's stiffnesses. Then, the chord's relative elongations ε_{pr} are calculated by (5) and the link load P_{pr} is obtained by (48a, 48b). Both the expressions (48), written for different chords, give exactly same result (the discrepancy is less than 10^{-11} %) meaning correctness of the link load calculation for the given cable truss. The link loads, P_{pr}, must, however be compared with the $P_{pr,bound}$-values, which ensure that the full uniform load Q_{tot} is completely taken by the cable truss.

Finding $P_{pr,bound}$-values is performed by (49) given the mid-span vertical deflections of the truss ω_{ld}. The deflections are obtained by nonlinear Finite Element Method. They are taken from the graph (Fig. 10 in [50]): ω_{ld} = {0.110, 0.178, 0.260, 0.353, 0.453, 0.557, 0.655, 0.755} m. Because the deflections ω_{ld} have been obtained regardless the strength properties of the chords, the limiting deformation $\varepsilon_{cab,2}$ in (49) is substituted by the actual deformation of the bearer cable $\varepsilon_{ld,b}$ (5) given ω_{ld}.

Comparison of P_{pr}-values and $P_{pr,bound}$-values, which are derived from different conditions implied on the cable truss, are shown in Figs. 17 and 18. The discrepancy between the link loads is obtained as follows:

$$\rho = 200 \cdot \frac{|V_0 - V_{ref}|}{V_0 + V_{ref}} \%, \tag{57}$$

where V_0 and V_{ref} are the values to be compared.

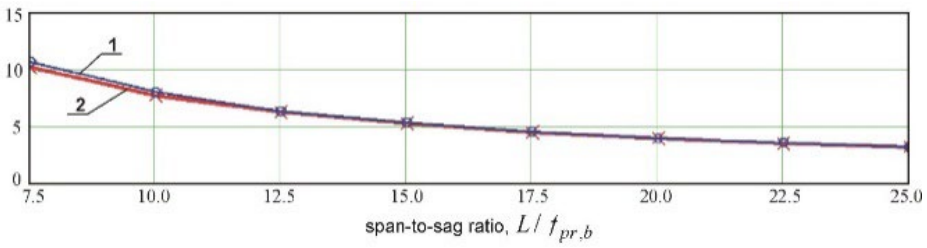

Figure 17. Link loads between the chords, kN/m: 1 – P_{pr}-values (48) given the stiffnesses of the chords; 2 – $P_{pr,bound}$-values (49) given the deflections under the load [50].

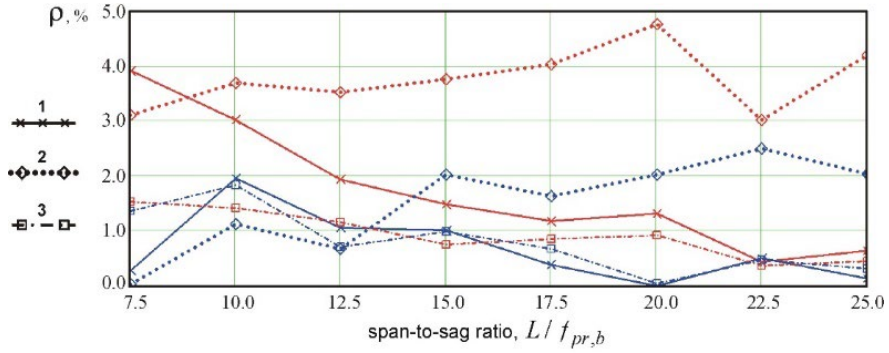

Figure 18. Percentage discrepancies ρ: 1 – discrepancies between the link loads $P_{pr,bound}$ and P_{pr}; 2 – discrepancies between the axial forces in the bottom chord; 3 – discrepancies between the axial forces in the top chord; red color is for the symmetric cable truss, while blue color is for non-symmetric one.

Fig. 18 shows that the discrepancies between the link loads do not exceed 4 % meaning that the cable truss is in equilibrium given the chord's stiffnesses, the external load and the corresponding deflections.

Considering the shallow shape of the chords, the horizontal components of the cable forces, H_b and H_t, are compared with the axial forces in the chords:

$$N_b = EA_r \cdot \varepsilon_{ld,r}; \tag{58a}$$

$$N_t = EA_b \cdot \varepsilon_{ld,b}, \tag{58b}$$

where N_b and N_t are the forces in the bottom and the top chords of the truss; ε_{ld} are the relative elongations of the chords given the deflection of the truss under load $\omega_{\lim}$ (5).

The horizontal components of the cable force are taken from the graphs (Figs. 8 and 9 in [50]). The comparison of the forces is shown in Figs. 18 and 19.

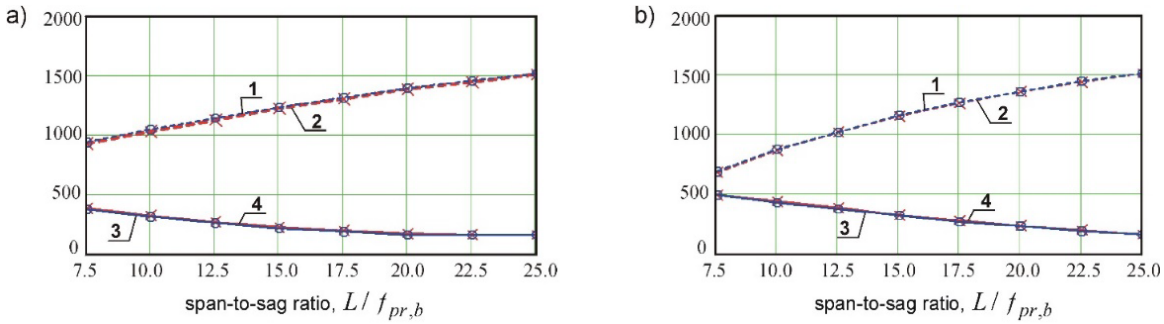

Figure 19. Axial forces and horizontal components of the forces, kN: a, b – symmetric and non-symmetric cable trusses, respectively; 1, 2 – N_t and H_t in the top chord; 3, 4 – N_b and H_b in the bottom chord.

Non-symmetric cable truss of the 60 meters span is also considered. Different span-to-sag ratios are adopted for the bearer chord $\left(L/f_{pr,b}\right)_j$, $j=[1...8]$, while for the restraining chord the constant ratio is taken: $L/f_{pr,r}$ = 25 [50]. The initial horizontal component of pretension of the restraining chord is $H_{0,b}$ = 600 kN, while for the bearer chord it is calculated by the following expression: $H_{0,t} = H_{0,b} \cdot f_{pr,r} / f_{pr,b}$. Mid-span vertical deflections of the truss are taken from the graph (Fig. 13 in [50]): $\omega_{\lim}$ = {0.162, 0.255, 0.342, 0.444, 0.531, 0.612, 0.689, 0.751} m.

Comparison of P_{pr} and $P_{pr,bound}$-values (48, 49) given the deflection $\omega_{\lim}$ is shown in Fig. 18. Comparison of the forces taken from the graphs (Figs. 11 and 12 in [50]) is shown in Figs. 18 and 19.

Figs. 18 and 19 show good agreement with the results [50] under uniformly distributed load acting on the entire span of the truss.

Influence of the load acting on a half of the span is also considered in [50]: Q_L = 8.91 kN/m and Q_R = 0.0.The span of the truss, L, is 60 m. The rises of the chords are the following: $f_{pr,b}$ = $f_{pr,r}$ = 4.02 m. The initial horizontal components of pretension of the chords are the following: $H_{0,b}$ = $H_{0,t}$ = 588.603 kN. The modulus of elasticity of the cables is E_{cab} = 1.48135·10^8 kN/m^2. Cross section areas of the chords are the following: A_b = 2.0·10^{-3} m^2 and A_r = 1.3·10^{-3} m^2.

The initial rise of the bearer chord is obtained by (39) given the pretension and the stiffness properties: $f_{0,b}$ = 3.66 m. Thus, the deflection of the truss at the stage of the pre-stressing is the following (1a): $\Delta f_{pr} = f_{0,b} - f_{pr,b} =$ –36 m.

The overall displacements of the truss under the loads Q_L and Q_R are obtained by minimizing (36): Δf = –0.5 m and $\Delta f_{1/4}$ = –0.72 m. Thus, the displacements of the truss at the center and at the quarter points of the span are the following: $\omega = \Delta f_{pr} - \Delta f =$ 0.14 m and $\omega_{1/4} = 0.75 \cdot \Delta f_{pr} - \Delta f_{1/4} =$ = 0.45 m. Considering the graph (Fig. 7 in [50]) the corresponding displacements are 0.146 m and 0.459 m. The discrepancies (57) are the following: 4.2 % and 2.0 %.

The comparison implemented in the present clause shows good agreement with the results by the other authors obtained numerically and by using the Finite Element Method.

4. Conclusions

1. The cable roof stiffened with a girder and enveloped with a flexible membrane is considered.
2. The polymer membrane is included into the structural model of the roof by using membrane-simulating element. The numerical technique for estimating the effective stiffness and the allowable relative deformation of the element is proposed.
3. The design clearances are proposed for the structural enhancement. The clearances, being the means of the passive structural adaptation, allow exempting the stiffening girder from uniformly distributed external loads, which are fully sustained by the cable truss. The girder, in turn, mitigates kinematic displacements brought about by non-uniform impacts. The calculating technique for splitting the non-uniform load between the cable truss and the girder is proposed.
4. The computational approach for structural analysis of the roof is proposed. The approach is based on the limit states analysis, which is mandatory for the design practice in Russian Federation.
5. Estimation of the allowable deformations of the roof at the pre-stressing and operational phases is proposed. The expressions for the axial stiffnesses of the cable chords, the design clearances and the link load between the chords at the pre-stressing stage are proposed under the conditions of reaching the allowable deformation and full use of the strength properties.
6. The work contributes to the development of hybrid building constructions, which consist of high-strength flexible cables, polymer membranes and rigid elements made of ordinary structural steel. It facilitates the practical realization of the hybrid roofs by providing the initial data for the conceptual design stage. The results of the present work allow to validate structural models and to verify the results obtained by numerical methods of structural analysis.

References

1. Bridgens, B.N., Gosling, P.D., Birchall, M.J.S. Tensile fabric structures: concepts, practice and developments. The Structural Engineer. 2004. 82 (14). Pp. 21–27.
2. Barozzi, M., Viscuso, S., Zanelli, A. Design novel covering system for archaeological areas. Proceedings of VII International Conference on textile composites and inflatable structures. Structural membranes 2015. 2015. 105–114.
3. Goppert, K. High tension tensile architecture. New stadium projects. Proceedings of VI International Conference on textile composites and inflatable structures. Structural membranes 2013. 2013. Pp. 21–26.
4. Llorens, J.I. Structural membranes for urban spaces. Proceedings of VII International Conference on textile composites and inflatable structures. Structural membranes 2015. 2015. Pp. 133–144.
5. Llorens, J., Zanelli, A. Structural membranes for refurbishment of the architectural heritage. Procedia Engineering. 2016. 155. Pp. 18–27. DOI: 10.1016/j.proeng.2016.08.003

6. Viscuso, S., Dragoljevic, M., Monticelli, C., Zanelli, A. Finite-element analysis and design optioneering of an emergency tent structure. Proceedings of the TensiNet Symposium. Softening the Habitats. 2019. Pp. 208–219.
7. Fangueiro, R., Rana, S. Towards high performance and multi-functional structural membranes using advanced fibrous and textile materials. Proceedings of VII International Conference on textile composites and inflatable structures. Structural membranes 2015. 2015. Pp. 296–305.
8. Wagner, R. Bauen mit Seilen und Membranen. Beuth Verlag GmbH. Berlin, Germany, 2016. 517 p.
9. Mushchanov, V., Rudneva, I., Priadko, Yu. Intense-deformed condition of suspended system of bending-rigid fibers at the account of pliability of supports. Metal Constructions. 2012. 18 (1). Pp. 5–16.
10. Arellano, H., Gomez, R., Tolentino, D. Parametric analysis of multi-span cable-stayed bridges under alternate loads. The Baltic Journal of Road and Bridge Engineering. 2019. 14 (4). Pp. 543–567. DOI: 10.7250/bjrbe.2019-14.457
11. Al-Rousan, R. The impact of cable spacing on the behavior of cable-stayed bridges. Magazine of Civil Engineering. 2019. 91 (7). Pp. 49–59. DOI: 10.18720/MCE.91.5
12. Mushchanov, V., Protopopov, I., Korsun, O., Garifullin, M. Definition of the rational geometry of the cable-beam cover over stadium tribunes. Procedia Engineering. 2015. 117. Pp. 1001–1012. DOI: 10.1016/j.proeng.2015.08.209
13. Yegorov, V.V., Aleksashkin, Ye.N. Predvaritelno-napryazhennaya shprengelnaya ferma [Pre-stressed strutted truss]. Patent RF no. 2169243, 1999.
14. Voyevodin, A.A. Predvaritelno-napryazhennyye sistemy elementov konstruktsiy [Pre-stressed systems of structural elements]. Moskva: Stroyizdat, 1989. 304 str.
15. Liew, J.Y.R., Punniyakotty, N.M., Shanmugam, N.E. Limit-state analysis and design of cable-tensioned structures. International Journal of Space Structures. 2001. 16 (2). Pp. 95–110. DOI: 10.1260/0266351011495205
16. Llorens, J. Detailing masts. Proceedings of the IASS Annual Symposium. Structural membranes 2019. 2019. Pp. 359–366.
17. Goremikins, V., Rocens, K., Serdjuks, D. Cable truss analyses for prestressed suspension bridge. Proceedings of VIII International DAAAM Baltic Conference. Industrial Engineering. 2012. Pp. 45–50.
18. Goremikins, V., Rocens, K., Serdjuks, D. Decreasing of displacements of prestressed cable truss. International Journal of Civil and Environmental Engineering. 2012. 6 (3). Pp. 228–236.
19. Goremikins, V., Rocens, K., Serdjuks, D. Cable truss analyses for suspension bridge. Proceedings of 11 International Scientific Conference. Engineering for Rural Development. 2012. Pp. 228–233.
20. Habraken, A.P.H.W., Sleddens, W., Teuffel, P. Adaptable lightweight structures to minimize material use. Proceedings of VI International Conference on textile composites and inflatable structures. Structural membranes 2013. 2013. Pp. 71–82.
21. Alekseytsev, A.V., Gaile, L., Drukis, P. Optimization of steel beam structures for frame buildings subject to their safety requirements. Magazine of Civil Engineering. 2019. 91 (7). Pp. 3–15. DOI: 10.18720/MCE.91.1
22. Serpik, I.N., Alekseytsev, A.V. Protivoavariynaya stalnaya balochnaya konstruktsiya [Emergency steel beam structure]. Patent RF no. 2556761, 2014.
23. Mikhailov, V.V., Chesnokov A.V., Dolmatov I.V. Pre-stressed cable truss with stiffening girder and design clearance: development and analysis. Proceedings of the TensiNet Symposium. Softening the Habitats. 2019. Pp. 58–70.
24. Freire, A.M.S., Negrao, J.H.O., Lopes, A.V. Geometrical nonlinearities on the static analysis of highly flexible steel cable-stayed bridges. Computers and Structures. 2006. 84 (31–32). Pp. 2128–2140. DOI: 10.1016/j.compstruc.2006.08.047
25. Greco, L., Impollonia, N., Cuomo, M. A procedure for the static analysis of cable structures following elastic catenary theory. International Journal of Solids and Structures. 2014. 51. Pp. 1521–1533. DOI: 10.1016/j.ijsolstr.2014.01.001
26. Coarita, E., Flores, L. Nonlinear analysis of structures cable - truss. International Journal of Engineering and Technology. 2015. 7 (3). Pp. 160–169. DOI: 10.7763/IJET.2015.V7.786
27. Nuhoglu, A. Nonlinear analysis of cable systems with point based iterative procedure. Scientific Research and Essays. 2011. 6 (6). Pp. 1186–1199.
28. Xu, J., Zhang, Y., Yu, Q., Zhang, L. Analysis and design of fabric membrane structures: a systematic review on material and structural performance. Thin-Walled Structures. 2022. 170. Pp. 1–17. DOI: 10.1016/j.tws.2021.108619
29. Nunes, E., Sousa, J.B.M, Baier, B., Freitas, A.M.S. Membrane roof for an amphitheater in Brazil: searching for the optimal design. International Journal of Space Structures. 2015. 30 (3-4). Pp. 261–271. DOI: 10.1260/0266-3511.30.3-4.261
30. Strobel, D., Singer, P., Holl, J. Analytical formfinding. International Journal of Space Structures. 2016. 31 (1). Pp. 52–61. DOI: 10.1177/0266351116642076
31. Tran, H.C., Lee, J. Advanced form-finding for cable-strut structures. International Journal of Solids and Structures. 2010. 47 (14–15). Pp. 1785–1794. DOI: 10.1016/j.ijsolstr.2010.03.008
32. Lang, R., Nemec, I. Form-finding of shell and membrane structures. Proceedings of VIII International Conference on textile composites and inflatable structures. Structural membranes 2017. 2017. Pp. 303–310.
33. Llorens, J.I. Appropriate design of structural membranes. Proceedings of X International Conference on textile composites and inflatable structures. Structural membranes 2021. 2021. DOI: 10.23967/membranes.2021.008
34. Machacek, J, Jermoljev, D. Steel structures in interaction with non-metallic membranes. Journal of Civil Engineering and Management. 2017. 23 (3). Pp. 368–377. DOI: 10.3846/13923730.2015.1128482
35. Stroebel, D., Holl, J. On the calculation of textile halls. Proceedings of X International Conference on textile composites and inflatable structures. Structural membranes 2021. 2021. DOI: 10.23967/membranes.2021.043
36. Hegyi, D. Numerical stability analysis of arch-supported membrane roofs. Structures. 2021. 29. Pp. 785–795. DOI: 10.1016/j.istruc.2020.11.025
37. Dinh, T.D., Rezaei, A., Linthout, T., Mollaert, M., Van Hemelrijck, D., Van Paepegem, W. A computational compensation method for fabric panels of tensioned membrane structures using a shape optimization method based on gradientless algorithms. International Journal of Solids and Structures. 2017. 112. Pp. 16–24. DOI: 10.1016/j.ijsolstr.2017.02.026
38. Haug, E., De Kermel, P., Gawenat, B., Michalski, A. Industrial design and analysis of structural membranes. International Journal of Space Structures. 2009. 24 (4). Pp. 191–204. DOI: 10.1260/026635109789968227
39. Wagner, R. Simplified design tools for single/double curved membranes and inflated cushions. International Journal of Space Structures. 2008. 23 (4). Pp. 233–241. DOI: 10.1260/026635108786959843

40. Grigorjeva, T., Juozapaitis, A. Revised engineering method for analysis of behavior of suspension bridge with rigid cables and some aspects of numerical modeling. Procedia Engineering. 2013. 57. Pp. 364–371. DOI: 10.1016/j.proeng.2013.04.048
41. Yan, H., Wei-ren, L. Static analysis of cable structure. Applied Mathematics and Mechanics (English Edition). 2006. 27 (10). Pp. 1425–1430. DOI: 10.1007/s10483-006-1015-y
42. Forster, B., Mollaert, M. European design guide for tensile surface structures. TensiNet. Brussel, Belgium, 2004. 354 p.
43. Chesnokov, A.V., Mikhaylov, V.V. Analysis of cable structures by means of trigonometric series. Proceedings of VIII International Conference on textile composites and inflatable structures. Structural membranes 2017. 2017. Pp. 455–466.
44. Bridgens, B., Birchall, M. Form and function: the significance of material properties in the design of tensile fabric structures. Engineering Structures. 2012. 44. Pp. 1–12. DOI: 10.1016/j.engstruct.2012.05.044
45. Gosling, P.D., Bridgens, B.N., Albrecht, A., Alpermann, H., Angeleri, A., Barnes, M., Bartle, N., Canobbio, R., Dieringer, F., Gellin, S., Lewis, W.J., Mageau, N., Mahadevan, R., Marion, J.M., Marsden, P., Milligan, E., Phang, Y.P., Sahlin, K., Stimpfle, B., Suire, O., Uhlemann, J. Analysis and design of membrane structures: results of a round robin exercise. Engineering Structures. 2013. 48. Pp. 313–328. DOI: 10.1016/j.engstruct.2012.10.008
46. Lightweight structure design. Easy. [Online]. URL: https://www.technet-gmbh.com/fileadmin/user_upload/technet/Produktinformationen/Easy/Easy_ProductBrochure.pdf. (date of application: 08.11.2022).
47. Chesnokov, A.V., Mikhailov, V.V., Dolmatov, I.V. The influence of material aging on the structural behavior of a flexible roof with a polymer membrane shell. Computer Methods in Materials Science. 2021. 21 (1). Pp. 13–24. DOI: 10.7494/cmms.2021.1.0748
48. European technical assessment. PFEIFER wire ropes. ETA-11/0160. [Online]. URL: https://www.pfeifer.info/out/assets/PFEIFER_WIRE-ROPES_TECHNICAL-APPROVAL-ETA-11-0160_EN.PDF. (date of application: 08.11.2022).
49. Harris, B. Engineering composite materials. The Institute of Materials. London, 1999. 194 p.
50. Kmet, S., Kokorudova, Z. Nonlinear closed-form computational model of cable trusses. International Journal of Nonlinear Mechanics. 2009. 44 (7). Pp. 735–744. DOI: 10.1016/j.ijnonlinmec.2009.03.004

Information about the authors:

***Andrei Chesnokov**, PhD in Technical Sciences*
ORCID: https://orcid.org/0000-0003-3687-0510
E-mail: andreychess742@gmail.com

***Vitalii Mikhailov**, Doctor of Technical Sciences*
ORCID: https://orcid.org/0000-0001-8274-9346
E-mail: mmvv46@rambler.ru

Received: 28.09.2022. Approved after reviewing: 09.07.2024. Accepted: 12.07.2024.